PREDICTION OF SOME TURBULENT FLOWS USING UPWIND AND HYBRID DISCRETISATION SCHEMES AND THE TWO-EQUATION TURBULENCE MODEL

TAHIR KARASU*, P. ROY CHOUDHURY and M. GERSTEIN

Department of Mechanical Engineering
University of Southern California
Los Angeles, California 90089

SUMMARY

The paper presents the use of a numerical solution procedure for the prediction of steady, incompressible and two-dimensional turbulent flow in a pipe, in sudden expansions in pipes, and over a backward-facing step using upwind and hybrid discretisation schemes.

The numerical procedure employs a two-equation turbulence model, which entails the solution of two differential equations of transport for characteristics of turbulence; namely, the kinetic energy of turbulence and its rate of dissipation. The Reynolds stresses are related to the mean velocity gradients through a scalar turbulent viscosity, calculated from the above turbulence variables. In the near-wall regions, wall functions are employed. The predictions results from simultaneous solution of differential equations for conservation of mass and momentum, together with equations describing the transport of turbulence, by means of a finite-difference solution procedure.

The predictions obtained using upwind and hybrid discretisation schemes are compared with each other and with published experimental data. For flows in which recirculation is present, the use of hybrid scheme results in closer agreement with measurements. In general, the predictions made are in good qualitative agreement with experiment.

1. INTRODUCTION

The present investigation is concerned with the prediction of some turbulent flows using upwind and hybrid discretisation schemes and the two-equation turbulence model[1,2]. Three flow situations have been considered; namely, axisymmetric developing turbulent flow through a pipe, axisymmetric turbulent flow through circular-sectioned sudden expansions, and finally plane turbulent flow over a backward-facing step. These flow situations are depicted in Fig. 3.

---

* *Assistant Professor, Department of Mechanical Engineering, Uludağ University, Bursa, Turkey.*

Developing turbulent pipe flow is basically a transition from a boundary layer type flow at the entrance to a fully developed flow downstream. The free stream in the inlet region is completely surrounded by the boundary layer, which by diffusion of momentum through laminar and turbulent mechanisms grows in thickness as the distance from the pipe inlet increases. The growing boundary layer accelerates the free stream which eventually loses its identity as the boundary layer merges with itself. Following the disappearance of the free stream, further changes occur in the velocity distribution and turbulence structure until the flow attains fully developed state.

Methods of analysis, whether analytical or numerical, for predicting turbulent pipe flow can be verified by comparison with experimental data reported in the literature (see, for example, Laufer[3], Lawn[4], Richman[5] and Taylor et al.[6]). The experimental work of Barbin and Jones[7] forms the basis for comparison in the present paper.

On the other hand, the flow field of axisymmetric sudden expansion in a pipe is a complicated phenomenon characterised by flow separation, flow recirculation, and flow reattachment. As illustrated in Fig. 3(b), such a flow field may be divided by a dividing surface into two main regions, one being the region of recirculation flow, the other being the region of main flow. The point at which the dividing surface strikes the wall is called the reattachment point. In the recirculation zone, the high adverse pressure gradient results in reverse flow and promotes instability and turbulence. Eddies generated in the recirculation zone and in the vicinity of the reattachment point can be considered as a highly concentrated source of turbulence. The subsequent convection, diffusion, and decay of the turbulent eddies have a dominant influence on the characteristics of mean flow.

Considerable experimental and theoretical works on turbulent flow through sudden expansions have been published in the literature. Among the interesting ones are the works of Chaturvedi[8], Moon and Rudinger[9], Yang and Yu[10], Novick et al.[11] and Rhode et al.[12,13] In the present study, the experimental measurements of Chaturvedi[8] and Moon and Rudinger[9] have been used to validate the upwind and hybrid discretisation schemes and the two-equation turbulence model.

Recently separation of turbulent flows has received a great deal of attention because of its practical importance; however, it is still far from well understood. In many real flows, separation of a boundary layer is followed downstream by reattachment of the separated layer to a solid wall. Flow over a backward-facing step considered in the present paper is a typical example of separated flows. The physical situation of this flow is revealed in Fig. 3(c), which consists of a single backward-facing step in a channel. The separation-reattachment process in this flow is characterised by complex interaction between the separated shear-layer and the adjacent flow. Downstream of reattachment, the flow returns slowly to the structure of an ordinary turbulent boundary layer.

Turbulent flow over a downstream-facing step has been studied both experimentally and theoretically by a number of researchers, among them are: Denham et al.[14], Atkins et al.[15], Thomas et al.[16], Taylor et al.[17] and Kim et al.[18] In the present context, the experimental data of Denham et al.[14] have been employed for comparison with the calculations.

The flows just described above have been predicted through the use of a mathematical model, which gives the local values of components of velocity, pressure and some useful properties of turbulence. The model comprises a set of non-linear partial differential equations, the simultaneous solution of which by means of a finite-difference solution procedure yields the local values of flow properties at all points in the flow domain. The Reynolds stresses arising from turbulence have been represented by a two-equation turbulence model, which entails the solution of two differential equations of transport for kinetic energy of turbulence and its rate of dissipation.

The remainder of the paper is now outlined. The next section provides the equations in a general form that govern turbulent flow. These equations are then discretised and the approximations made to model the convective terms are provided for the upwind and hybrid schemes. The two schemes are then applied to three turbulent flows in Section 4. Finally conclusions drawn from the present work are presented in Section 5.

2. THE MATHEMATICAL FORMULATION

2.1. The Equations

The time-averaged equations governing steady, incompressible two-dimensional flow in the cylindrical coordinate system can be conveniently cast into the following form:

$$\frac{\partial}{\partial x}[\rho u \phi] + \frac{1}{r} \frac{\partial}{\partial r}[\rho r v \phi] - \frac{\partial}{\partial x}[\Gamma_\phi \frac{\partial \phi}{\partial x}] - \frac{1}{r} \frac{\partial}{\partial r}[r \Gamma_\phi \frac{\partial \phi}{\partial r}] = S_\phi \tag{1}$$

in which ρ is the fluid density, u and v are the velocities in the axial (x) and radial (r) directions respectively; the general variable ϕ can stand for either of the two velocity components; and for $\phi = 1$, the above equation reduces to the continuity equation. Moreover, the general variable ϕ can represent a turbulence quantity, such as turbulence kinetic energy, k, and turbulence kinetic energy dissipation rate, ϵ. The Γ's and S's are respectively the exchange coefficient and source/sink terms associated with each ϕ-variable; the expressions for these quantities are given in Table 1. The equations (1) describe also motions in Cartesian coordinate system when r and ∂r are set equivalent to one and ∂y, respectively.

Table 1 — *Expressions for the Exchange Coefficients, Γ_ϕ and Source Terms, S_ϕ for Any Conserved General Property, ϕ.*

Conservation of	ϕ	Γ_ϕ	S_ϕ
Mass	1	0	0
Axial momentum	u	μe_{ff}	$-\frac{\partial p}{\partial x} + \frac{\partial}{\partial x}[\mu e_{ff} \frac{\partial u}{\partial x}] + \frac{1}{r} \frac{\partial}{\partial r}[r \mu e_{ff} \frac{\partial v}{\partial x}]$
Radial momentum	v	μe_{ff}	$-\frac{\partial p}{\partial r} + \frac{\partial}{\partial x}[\mu e_{ff} \frac{\partial u}{\partial r}] + \frac{1}{r} \frac{\partial}{\partial r}[r \mu e_{ff} \frac{\partial v}{\partial r}] - 2\mu e_{ff} \frac{v}{r^2}$
Kinetic energy	k	$\frac{\mu e_{ff}}{\sigma_k}$	$G_k - \rho \epsilon$
Dissipation rate	ϵ	$\frac{\mu e_{ff}}{\sigma_\epsilon}$	$\frac{\epsilon}{k}[C_1 G_k - C_2 \rho \epsilon]$

The use of time-mean equations and the isotropic effective-viscosity concept implied by Table 1, is complemented by equations of transport that determine the distribution of the properties of turbulence. It is to the model of turbulence that attention is now turned.

2.2. The Turbulence Model

The turbulence model employed in the present calculations is the k-ϵ model[1,2]; it necessitates the solution of two equations of transport for two turbulence quantities; namely turbulence kinetic energy, k, and its rate of dissipation, ϵ.

Knowledge of the local values of k and ϵ allows the evaluation of a local effective viscosity from which the turbulent shear stresses are calculated.

With reference to Table 1, the effective viscosity μe_{ff} is calculated by

$$\mu e_{ff} = \mu_\ell + \mu_t = \mu_\ell + C\mu\rho\,\frac{k^2}{\varepsilon} \qquad (2)$$

where ρ and μ_l are respectively the density and molecular viscosity. μ_t and μe_{ff} are respectively the turbulent and effective viscosities. The quantity $C\mu$ and the quantities C_1, C_2, σ_k and σ_ϵ appearing in Table 1, are the turbulence model constants. The values of which are given in Table 2, and are the same as those recommended by Launder and Spalding[2].

Table 2 — The Values of the Constants Used in the k-ε
Turbulence Model.

$C\mu$	C_1	C_2	σ_k	σ_ϵ
0.09	1.44	1.92	1.0	1.3

The generation rate of turbulence kinetic energy, G_k, is:

$$G_k = \mu_t\left\{ 2\left[\left(\frac{\partial u}{\partial x}\right)^2 + \left(\frac{\partial v}{\partial r}\right)^2 + \left(\frac{v}{r}\right)^2\right] + \left(\frac{\partial u}{\partial r} + \frac{\partial v}{\partial x}\right)^2 \right\} \qquad (3)$$

2.3. The Wall Functions

In the near-wall region, there is a steep variation in the fluid properties. To avoid the need for detailed calculations in these regions, algebraic relations are employed to relate the values of the dependent variables at a point on the wall to those at a point adjacent to the wall; a logarithmic layer is presumed to exist between these two points.

The wall functions employed in the present study are those recommended by Launder and Spalding[2], they are:

velocity parallel to wall

$$\frac{U_P}{\left(\frac{\tau_w}{\rho}\right)}\, C\mu^{\frac{1}{4}} k_P^{\frac{1}{2}} = \frac{1}{\kappa}\, \ln\left(E\, y_P\, \frac{\rho C\mu^{\frac{1}{4}} k_P^{\frac{1}{2}}}{\mu_\ell} \right) ; \qquad (4)$$

turbulence energy dissipation rate

$$\varepsilon_P = \frac{C\mu^{3/4} k_P^{3/2}}{\kappa\, y_P} , \qquad (5)$$

in which U_p, k_p, and ϵ_p and y_p are the values of the velocity parallel to the wall, turbulence kinetic energy and dissipation rate of turbulence kinetic energy at a near wall point P, a distance y_p from the wall point w. At the wall point w, the shear stress, τ_w, is known or calculable; the constants E and κ are ascribed the values of 9.0 and 0.4 respectively.

2.4. The Finite Difference Discretisation

Equations (1) are solved, with their appropriate boundary conditions, by integrating them over finite-difference control volumes that form the physical integration domain considered; an example of the grid arrangement is depicted in Fig. 1 where it is seen that the grid is staggered so that velocity components are situated mid-way between the grid points. The pressure, viscosity and any general scalar variable such as

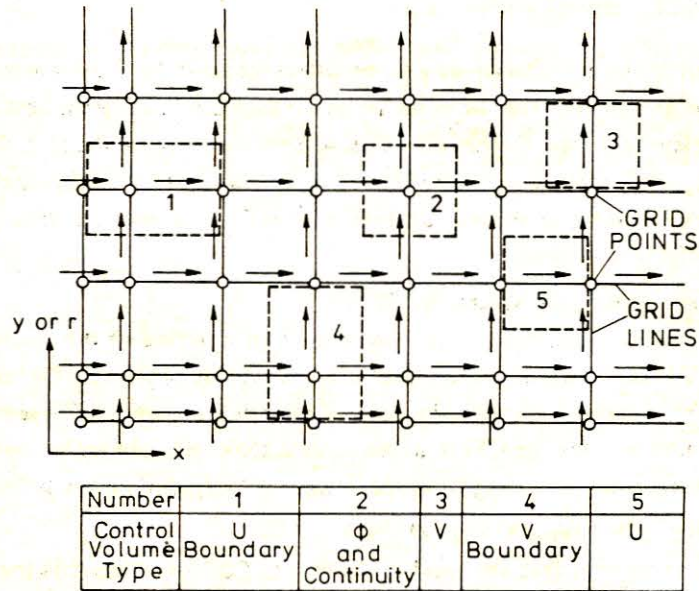| Number	1	2	3	4	5
Control Volume Type	U Boundary	ϕ and Continuity	V	V Boundary	U

Figure 1 — Control volume specification.

kinetic energy of turbulence, dissipation rate of turbulence kinetic energy are located at the grid points. The main advantage of this arrangement is that the pressure difference between two adjacent grid points becomes the natural driving force for the velocity component located between these grid points. Now, consider a single control volume for ϕ, as depicted in Fig. 2; integration of equation (1) over this control volume gives

$$\left[r\rho u\phi - r\Gamma_\phi \frac{\partial\phi}{\partial x}\right]_e A_e^\phi - \left[r\rho u\phi - r\Gamma_\phi \frac{\partial\phi}{\partial x}\right]_w A_w^\phi + \left[r\rho v\phi - r\Gamma_\phi \frac{\partial\phi}{\partial r}\right]_n A_n^\phi$$

$$- \left[r\rho v\phi - r\Gamma_\phi \frac{\partial\phi}{\partial r}\right]_s A_s^\phi = S_\phi r A_P^\phi \tag{6}$$

in which the A's denote cell-face areas at four points (e, w, n, s) located mid-way between the grid points.
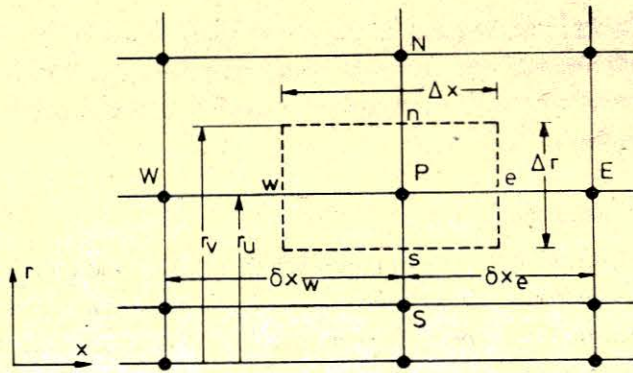
Figure 2 — Control volume for a scalar variable

The next step in the formulation of a finite-difference equation is the assumption of the variation of ϕ between any two grid points. The diffusion terms are formulated using the central difference scheme; and, since this is common practice, further attention will not be given to them. Attention is given to the convection terms (e.g., the $r\rho u\phi$ terms). Furthermore, the schemes that are used to approximate the convection terms are only applied to the convected variable (i.e., ϕ in Eq. (6)); the convecting velocity is discretised using the central — difference scheme.

i) The Central — Difference Scheme (CDS)

In the central-difference scheme, the value of ϕ at an interface of the control volume is taken as the average value of the ϕ's at the grid points that lie on either side of the interface of the control volume. For velocities that are low enough, central-difference scheme is recommended; however, it has been found that when the grid Peclet number ($u\triangle x/\Gamma$) is greater than 2, the coefficient matrix becomes non-diagonally dominant[19]. As a consequence, a semi-implicit-type numerical scheme, as normally used, becomes unstable.

ii) The Upwind — Difference Scheme (UDS)

This scheme recognizes that the weak point in the CDS formulation is the assumption that the convected property ϕ at an interface is the average of the ϕ's at the grid points that lie on either side of the interface, and it proposes a better resolution. That is, a piecewise-linear variation of ϕ between grid points is assumed for the diffusive flux, while for the convective flux the value of ϕ convected across an interface is taken to be the value of ϕ at the grid point on the upwind side of the face; for example, when the convective flux is calculated across the east face, e, of the control volume, the value of ϕ_e is expressed as[20]:

$$\phi_e = \begin{cases} \phi_P & \text{if} \quad U_e > 0 \ , \\ \phi_E & \text{if} \quad U_e < 0 \ . \end{cases} \tag{7}$$

This approximation overcomes the stability problem associated with the use of the CDS. In the present study, the upwind-difference scheme is also employed for velocities that are low enough (i.e., $P_e < 2$), even though CDS would be preferable.

iii) The Hybrid — Difference Scheme (HDS)

The hybrid-difference scheme, which was developed by Spalding[21], is a combination of both CDS and UDS; it permits the value of ϕ at an interface of the control volume to be calculated by allowing the CDS to prevail when $P_e < 2$ and UDS for $P_e > 2$; and for the latter situation the effect of the diffusion term in the general equation is assumed to be negligible (i.e., zero).

2.5. The Finite Difference Equations

By introducing the foregoing formulations for the ϕ-distributions at the interfaces of the control volume, the finite-difference representation of the general differential equation (1) can be formed. For two-dimensional flow, the finite-difference equations are of the following form:

$$\phi_P = \frac{C_N^\phi \phi_N + C_S^\phi \phi_S + C_E^\phi \phi_E + C_W^\phi \phi_W + S_U^\phi}{C_N^\phi + C_S^\phi + C_E^\phi + C_W^\phi - S_P^\phi} \tag{8}$$

in which C's are the coefficients which consist of contributions from convection and diffusion, the former being obtained with the help of the finite-difference scheme selected (i.e., CDS, UDS, HDS). The S's are components of the source term. Clearly, the C's and S's are uniquely formulated for each finite-difference scheme. It is to these formulations that attention is now turned.

i) The Upwind – Difference Scheme

The detailed derivation of the C's and S's for UDS and HDS schemes are given in Patankar[20]; here the results of manipulating the equations are presented. With reference to Fig. 2, the C's take the forms given below:

$$C_N^\phi = [[D_n^\phi , D_n^\phi - C_n^\phi]] \quad , \quad C_S^\phi = [[D_s^\phi , D_s^\phi + C_s^\phi]] \quad ,$$

$$C_E^\phi = [[D_e^\phi , D_e^\phi - C_e^\phi]] \quad , \quad C_W^\phi = [[D_w^\phi , D_w^\phi + C_w^\phi]] \tag{9}$$

in which

$$D_n^\phi = \frac{\Gamma_{\phi,n} r_n^\phi A_n^\phi}{\delta r_n} \quad , \qquad C_n^\phi = \rho_n v_n r_n^\phi A_n^\phi$$

$$D_e^\phi = \frac{\Gamma_{\phi,e} r_e^\phi A_e^\phi}{\delta x_e} \quad , \qquad C_e^\phi = \rho_e u_e r_e^\phi A_e^\phi \quad \text{etc.}$$

The brackets [[ ]] signify that the C's are assigned the maximum of the values contained within them.

The source term S_ϕ in equation (1) is integrated over the control volume shown in Fig. 2 and linearised to allow dependence on ϕ_p. The result is:

$$S_\phi (r_p \Delta x \Delta r) = S_u^\phi + S_P^\phi \phi_P \tag{10}$$

and Table 3 shows the appropriate S_u^ϕ and S_p^ϕ for each of the ϕ-values; S_p^ϕ must be negative to guarantee numerical stability. If there is no real dependence on ϕ_p, then S_p^ϕ is simply set to zero.

Table 3 — The Form of the Components of the Linearised Source Term.

ϕ	S_u^{ϕ}/V^{*}	S_P^{ϕ}/V
u	$-\frac{\partial p}{\partial x} + \frac{\partial}{\partial x}[\mu e_{ff}\frac{\partial u}{\partial x}] + \frac{1}{r}\frac{\partial}{\partial r}[r\mu e_{ff}\frac{\partial v}{\partial x}]$	0
v	$-\frac{\partial p}{\partial r} + \frac{\partial}{\partial x}[\mu e_{ff}\frac{\partial u}{\partial r}] + \frac{1}{r}\frac{\partial}{\partial r}[r\mu e_{ff}\frac{\partial v}{\partial r}]$	$-\frac{2\mu e_{ff}}{r^2}$
k	$1.5G_k + (C_2-1)\rho\epsilon$	$-\frac{(C_2\rho\epsilon + 0.5G_k)}{k}$
ϵ	$\frac{\epsilon}{k}[C_1G_k + (C_2-1)\rho\epsilon]$	$-\rho\frac{\epsilon}{k}(2C_2-1)$

* In this table, V stands for the cell control volume and G_k is defined in Eq. (3).

ii) The Hybrid — Difference Scheme

The source terms and the convection and diffusion coefficients for UDS given in the preceding sub-section are the same for HDS; however, the C's have different definitions as follows

$$C_N^{\phi} = [\![\; 0,\; D_n^{\phi} - 0.5C_n^{\phi},\; -C_n^{\phi}\;]\!] \quad ,$$

$$C_S^{\phi} = [\![\; 0,\; D_s^{\phi} + 0.5C_s^{\phi},\; C_s^{\phi}\;]\!] \quad ,$$

$$C_E^{\phi} = [\![\; 0,\; D_e^{\phi} - 0.5C_e^{\phi},\; -C_e^{\phi}\;]\!] \quad , \tag{11}$$

$$C_W^{\phi} = [\![\; 0,\; D_w^{\phi} + 0.5C_w^{\phi},\; C_w^{\phi}\;]\!] \quad .$$

3. THE NUMERICAL SOLUTION PROCEDURE

The numerical solution procedure employed to solve the finite-difference equations was the well-known SIMPLE algorithm[22,23]; this algorithm was embodied in the general two-dimensional computer code, named 2|E|FIX, of Pun and Spalding[24]. In this computer code the flow variables are calculated in a semi-implicit line-by-line fashion over a staggered finite-difference grid system (see Fig. 1). Owing to the semi-implicit nature of the code, under-relaxation factors are used. Since the present study is primarily concerned with the outcome of the calculations employing this code and not the code itself, readers who are interested in the details of the 2|E|FIX code may refer to Pun and Spalding[24], and Karasu[25].

4. THE RESULTS OF THE PREDICTIONS

4.1. The Physical Situations Considered

In this section, the results of the predictions are presented. Consideration is given to three turbulent flow situations:

i) axisymmetric developing turbulent flow through a pipe;

ii) axisymmetric turbulent flow through circular-sectioned sudden expansions; and

iii) plane turbulent flow over a backward-facing step.

The three physical flow situations considered are revealed in Fig. 3 with their appropriate physical quantities that characterise each flow situation. In the following, each flow situation is studied separately and in detail; and for flow situation (i) the UDS, for (ii) the UDS and HDS and for (iii) the HDS are evaluated in terms of accuracy and computational expense; this latter term implying the number of iteration cycles required by the computer code to attain a pre-specified level of convergence (i.e., summing all the terms in each equation over all control volumes in the computational domain and non-dimensionalising with respect to the influx of the quantity being considered).
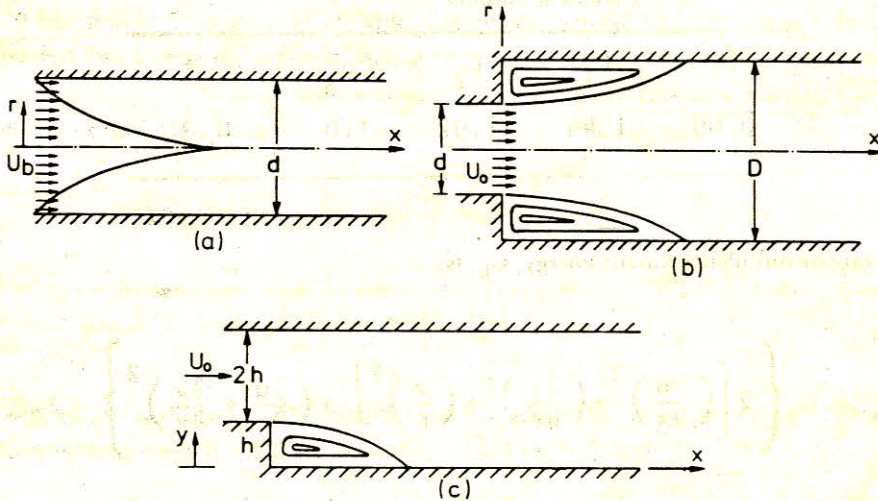
Figure 3 — Physical situations considered.

4.2. Turbulent Flow Through a Pipe

4.2.1. The physical situation considered

In this case the physical situation considered corresponds to the experimental situation of Barbin and Jones[7]. The physical situation and coordinate system employed for the predictions is sketched in Fig. 3(a).

Air enters the pipe with a uniform velocity profile, and the flow of air develops along the pipe. In the inlet region, the free stream is completely surrounded by the growing boundary layer and accelerates as the thickness of the boundary layer increases; it loses its identity downstream when the boundary layer thickness attains a value equal to the pipe radius. Following the disappearance of the free stream, further changes in the velocity distribution and structure of turbulence occur before a fully developed state is reached.

4.2.2. Boundary conditions

With reference to Fig. 3(a), the boundary conditions for the physical situation here considered are given below.

At the entrance to the pipe (i.e., $x/d = 0$), a uniform bulk velocity (U_b) corresponding to the experimental condition is prescribed, while the radial velocity v is specified as zero. The distribution of the turbulence quantities is prescribed by reference to the pipe radius and the bulk inlet velocity (i.e., $k = 0.03U_b^2$, $\epsilon = C_\mu k^{3/2}/0.03R$). At the exit of the pipe, a condition of zero axial gradient is specified for all dependent variables (i.e., $\partial\phi/\partial x = 0$) except radial velocity v, which is set equal to zero. At the pipe wall u

and v are set equal to zero. At the symmetry axis, v is set equal to zero, and a condition of zero radial gradient is specified for all dependent variables, i.e., $\partial\phi/\partial r = 0$.

For the components of velocity in the near-wall region, the specified boundary conditions are the components of the wall-shear stress in the direction of the velocity. This component is identically zero for the velocity component normal to the wall, and is calculated from the wall functions described in Section (2. 3) for the other velocity component.

The value of k for the near-wall grid point is calculated from the regular k-balance equation using the wall functions described in Section (2. 3), while the value of ϵ is fixed according to Eq. (5).

4.2.3. Some computational details

Since the flow in the pipe is axisymmetric, computations were performed only for half of the pipe diameter. The computational grid used possessed 34x12 grid points in the x- and r-directions, respectively. It was distributed non-uniformly in both x- and r-directions, with particularly more grid points placed in the near wall region where steep gradients of dependent variables were expected. The length of the calculation domain extended 48 diameters downstream from the pipe inlet. For this grid a well-converged solution was attained after 25 iteration cycles of the computational flow domain.

The convergence criterion was obtained by specifying that the residuals to each equation, defined by

$$R_\phi = \frac{\displaystyle\sum_{\text{all cells}} (\text{convection} + \text{diffusion} + \text{source})}{\text{inlet flux of } \phi}$$

to be less than 10^{-3} for all equations; to obtain this level of convergence required (for the grid size quoted above) 43 secs. central processing unit time on Pokey computer of TOPS-20 timesharing operating system of the University of Southern California.

For this case the under-ralaxation factors used in the predictions for u, v, k, ϵ, p and μe_{ff} were 0.6, 0.6, 0.8, 0.8, 0.5 and 0.3, respectively.

4.2.4. Presentation and discussion of results

The results of predictions for this case were obtained using the UDS scheme, and are presented in Figs. 4 to 6 for a Reynolds number of 3.88×10^5. The predictions are compared with experimental data of Barbin and Jones[7].

Figure 4 shows the development of radial profiles of axial velocity along the pipe in dimensionless form u/u_b, and radial distance r/R. From the figure it is seen that the predicted profiles compare favourably with the corresponding experimental ones, although some discrepancies are observed in the core region at dimensionless axial locations x/d = 28.5 and 40.5. The discrepancies in this region are probably generated by the UDS scheme, which, for velocities that are large enough, neglects the diffusion (see, for example, S.V. Patankar[20], and M.A. Leschziner[26]).

The development of the axial velocities in the downstream direction, at various axial locations is revealed in Fig. 5. It is noted that close to the wall, the predicted axial velocities develop far more rapidly than in the core region of the pipe. This behaviour is in accord with the experimental findings of Barbin and Jones[7]. The predicted axial velocities, like the experimental ones of Barbin and Jones[7], did not attain the fully developed state at the last axial location in the pipe; a longer length is needed to reach the fully developed state.

In Fig. 6, the wall-shear stress distributions in dimensionless form τ_w/τ_{wd}, and axial distance x/d, are displayed. Here, the wall-shear stress is non-dimensionalised with respect to the wall-shear stress, τ_{wd}, at axial location x/d = 15, where it attained its fully developed value. Agreement between the predicted and experimental distributions is reasonable.
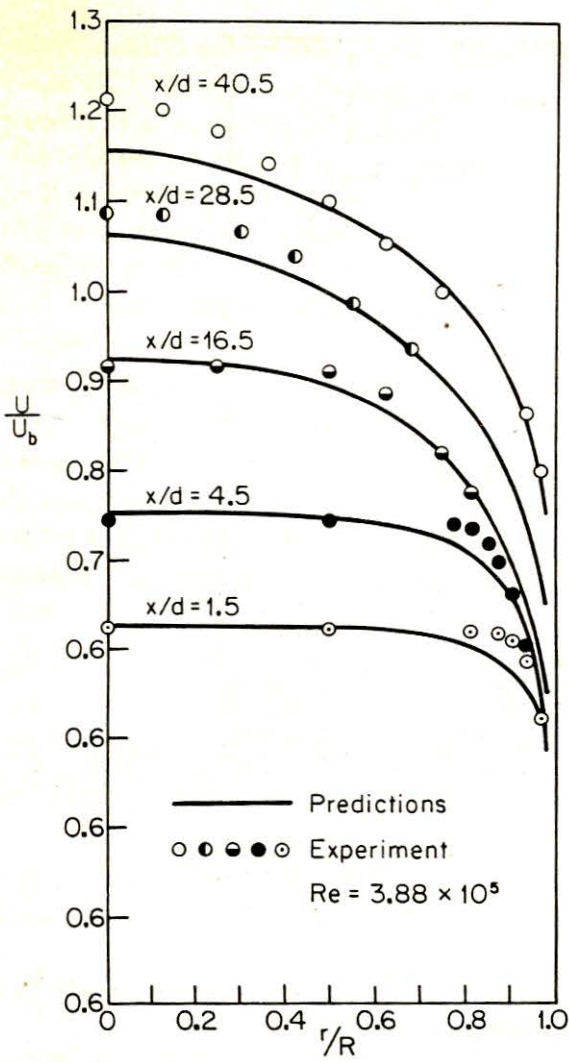
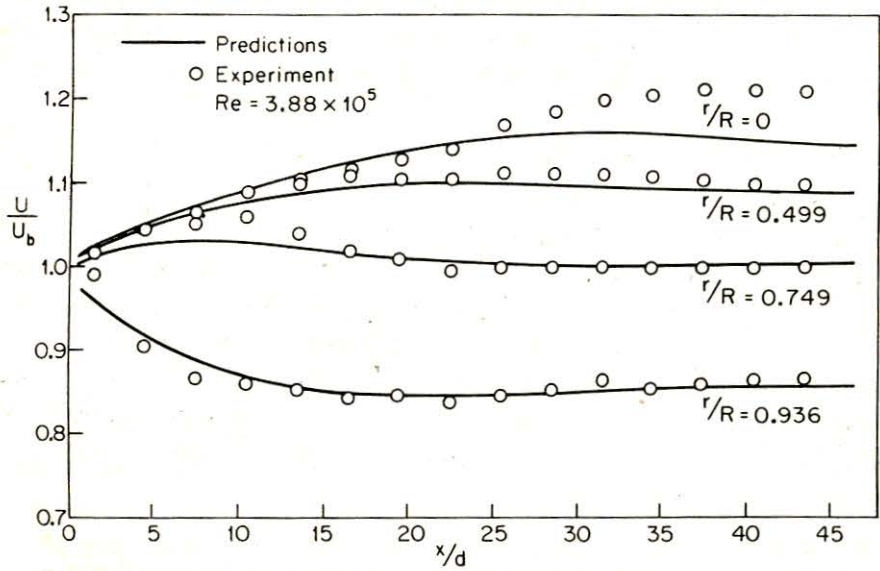Figure 4 — Comparison of predicted axial velocity profiles with experimental data of Barbin and Jones[7].

Figure 5 — Comparison of predicted variation of axial velocity along pipe with experimental data of Barbin and Jones[7].
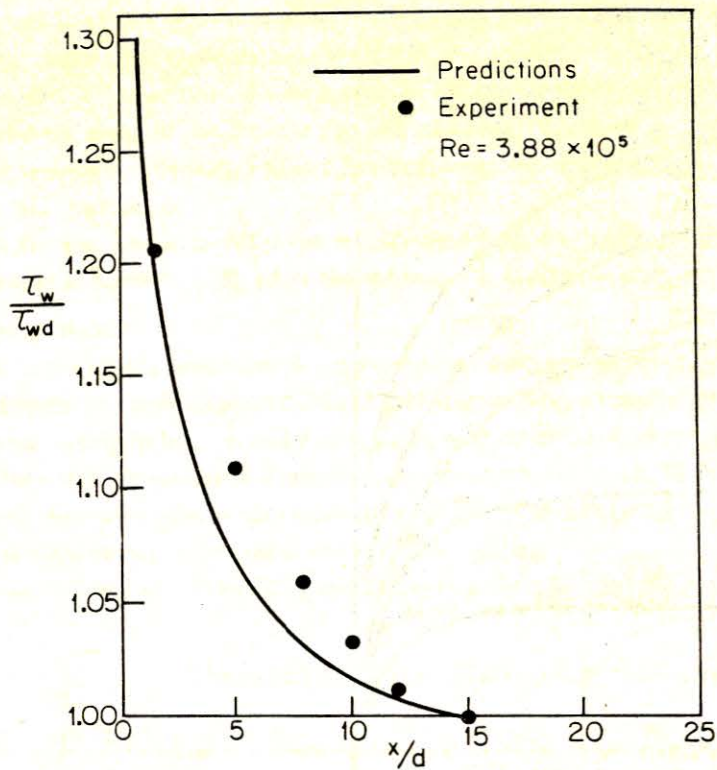
Figure 6 — Comparison of predicted dimensionless wall-shear stress with experimental data of Barbin and Jones[7].

For this case the 34x12 grid employed proved adequate and local refinements of the grid did not result in an appreciable increase in the accuracy of the predictions.

Computations were also performed, with the same 34x12 grid size, using the HDS scheme; however, the results obtained were exactly the same as those for UDS scheme. For this reason they were not presented.

To test further the performance of UDS and HDS schemes, more severe flow situations are required. That is, flow situations that possess recirculation zones in which flow reversals are present. It is for this reason that attention is turned to the turbulent flow through sudden expansions in pipes.

4.3. Axisymmetric Turbulent Flow Through Sudden Expansions in Pipes

4.3.1. The physical situation considered

The physical and flow configuration of the sudden expansion pipe flow is revealed in Fig. 3(b). Two types of flow configurations were studied: one with an expansion ration of $D/d = 2$, and the other of 1.428. The former corresponds to the experimental situation of Chaturvedi[8], while the latter corresponds to the experimental situation of Moon and Rudinger[9]. As seen from the figure, the flow is assumed symmetric about the centreline axis. Immediately after the step, and bounded by the larger diameter pipe, there is a recirculation zone in which flow reversal is present. The main flow in the core region, which is initially surrounded by the inner surface of the recirculation zone, gradually adjusts itself until it attains the fully developed condition further downstream.

4.3.2. Boundary conditions

The boundary conditions for the two types of flow configurations studied are given in the following.

At the inlet to the sudden expansion pipe, a uniform mean axial velocity (U_0) corresponding to the experimental condition is specified, while the radial velocity v is set equal to zero. The turbulence kinetic

energy k and its dissipation rate ϵ are assigned uniform values (i.e., $k = 0.005U_o^2$, $\epsilon = C_\mu k^{3/2}/0.03(D/2)$, where U_o is the mean axial velocity at the inlet). At the side-wall, velocity components u and v are put equal to zero. At the exit of the sudden expansion pipe, where the flow is parabolic, a condition of zero axial gradient is prescribed for all dependent variables (i.e., $\partial\phi/\partial x = 0$) except radial velocity v, which is set equal to zero. At the top wall u and v are put equal to zero. At the axis of symmetry, a condition of zero radial gradient is specified for all dependent variables (i.e., $\partial\phi/\partial r = 0$), while radial velocity v is set to zero.

As described in sub-section (4.2.2), the values of k and ϵ at the nearwall grid points are calculated using the wall functions described in Section (2.3).

4.3.3. Some computational details

The computational finite-difference grid distribution for experimental flow configuration of Chaturvedi[8] is depicted in Fig. 7. It possesses 26x20 grid points in the x- and r-directions, respectively. Its distribution is non-uniform in both x- and r-directions, with more grid points spaced in the near-wall regions and recirculation zone of the sudden expansion where steep gradients of dependent variables are expected. The length of the computational domain in the streamwise direction was taken to be 12.5D
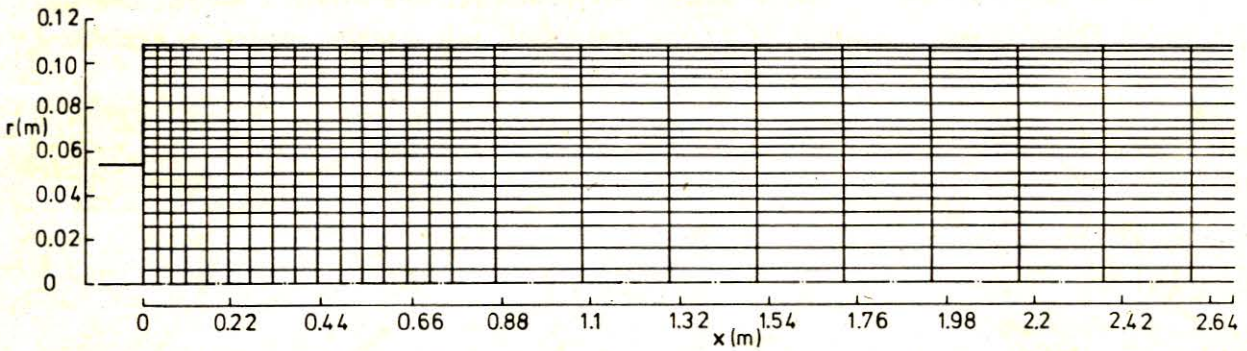

Figure 7 — Finite-difference grid distribution for axisymmetric sudden expansion of Chaturvedi[8]. Expansion ratio: D/d = 2.

(D is the diameter of the sudden expansion pipe), so that the exit boundary conditions had no effect upon the details of the flow. On the other hand, the finite difference grid used for experimental flow configuration of Moon and Rudinger[9] had 33x18 grid points in the x- and r-directions, respectively; and was distributed non-uniformly in the respective directions. The length of the calculation domain for this grid extended 18D downstream from the inlet section of the sudden expansion pipe.

For 26x20 grid using the HDS scheme, a well-converged solution was achieved after 475 iteration cycles, and the computational time required was 14.45 min. on Pokey computer of TOPS-20 timesharing operating system of the University of Southern California. For the same grid size employing the UDS scheme, a well-converged solution was obtained after 456 iteration cycles, and the computational time required was 11.25 min. on the same computer. On the other hand, for 33x18 grid size employing the HDS scheme, a well-converged solution was reached after 398 iteration cycles, and the required computational time was 8.033 min. For the same grid size using the UDS scheme, the number of iteration cycles performed to obtain a well-converged solution was 447, and the computational time needed was 8.5 min. Convergence criteria were again chosen as 10^{-3} for each equation.

For the grid sizes quoted above, the under-relaxation factors employed in the calculations for u, v, k, ϵ, p and μe_{ff} were 0.3, 0.3, 0.5, 0.5, 0.5 and 0.3, respectively.

4.3.4. Presentation and discussion of results

In this case the results are presented for two sudden expansion configurations of different expansion ratios.

The first flow configuration, which represents the experimental situation of Chaturvedi[8], has an expansion ration $D/d = 2$. The computations were performed for a Reynolds number ($Re = u_o d / \nu$, where u_o is the mean axial velocity in the smaller pipe) equal to 2.2×10^5 using a 26x20 grid. This grid, shown in Fig. 7, was considered adequate to predict the flow. For this reason, grid refinement tests were not carried out.

Figs. 8(a) and (b) display the predicted radial profiles of axial velocity obtained using the HDS and UDS schemes, and their comparisons with the experimental measurements of Chaturvedi[8], in terms of dimensionless form u/u_o, and radial distance r/D, at various axial locations in the sudden expansion pipe. From the figures it is seen that the predicted profiles exhibit good qualitative agreement with the corresponding measured ones, and that the agreement between the predicted and measured profiles at downstream axial locations becomes better. Furthermore, it is noticed that the predicted profiles obtained using the HDS scheme are in closer agreement with the corresponding experimental ones than those obtained using the UDS scheme. Also the discrepancies between the predictions made using the HDS and UDS schemes diminish as the flow develops along the sudden expansion pipe; and, at axial locations $x/D = 4$ and 11 both predictions coincide. However, as observed in Fig. 8(a), the length of the recirculation zone is underpredicted, and the predicted rate of spread of the round jet is too high, i.e., the predicted thickness of the recirculation zone is too small. The source of this problem is a limitation of the present k-ϵ turbulence model. The model does not account for the time lapse between extra turbulent energy being supplied and the effect being felt in the dissipating motions.
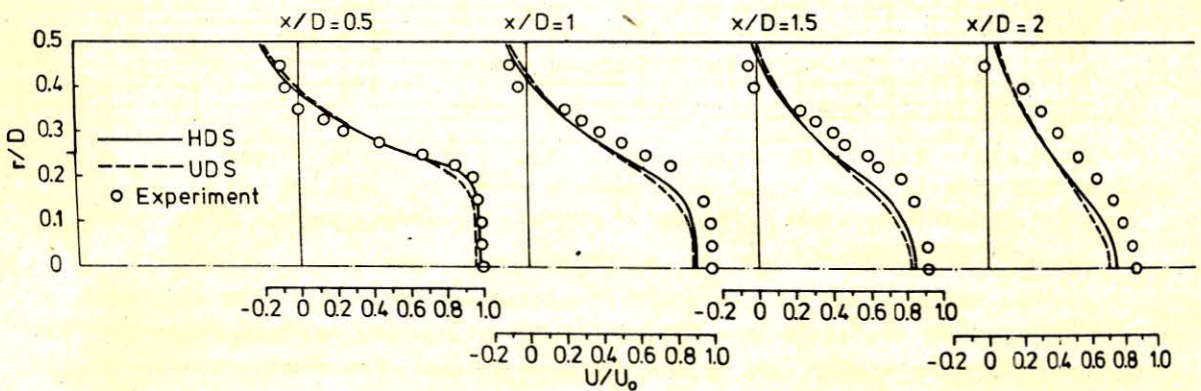

Figure 8 (a) — Comparison of predicted radial profiles of axial velocity with experimental data of Chaturvedi[8] for an axisymmetric sudden expansion. Expansion ratio: $D/d = 2$.
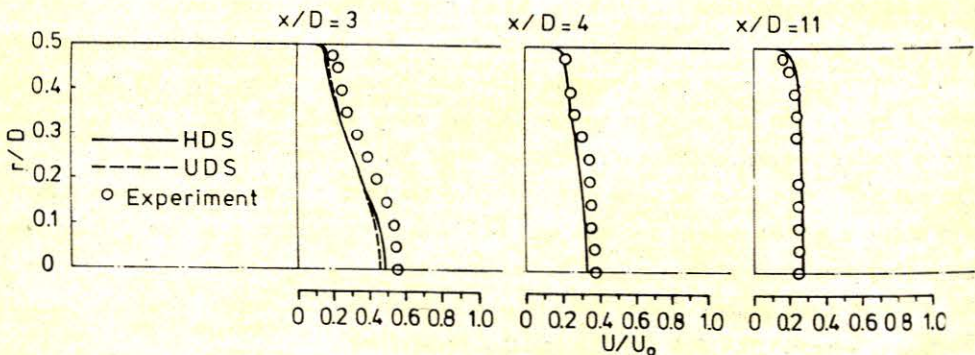

Figure 8 (b) — Comparison of predicted radial profiles of axial velocity with experimental data of Chaturvedi[8] for an axisymmetric sudden expansion. Expansion ratio: $D/d = 2$.

The second flow configuration, which corresponds to the experimental situation of Moon and Rudinger[9], possesses an expansion ratio $D/d = 1.428$. The calculations were made for a Reynolds number ($Re = u_o d / \nu$, where u_o is the centre-line velocity of fully developed turbulent velocity profile in the smaller pipe at the entrance of the larger one) of about 2.8×10^5 employing a 33x18 grid. This grid was considered adequate for the calculations.

The predicted radial profiles of axial velocity obtained by the use of the HDS scheme are displayed in Fig. 9 as a function of the dimensionless distance from the wall, y/D, at various axial locations in the
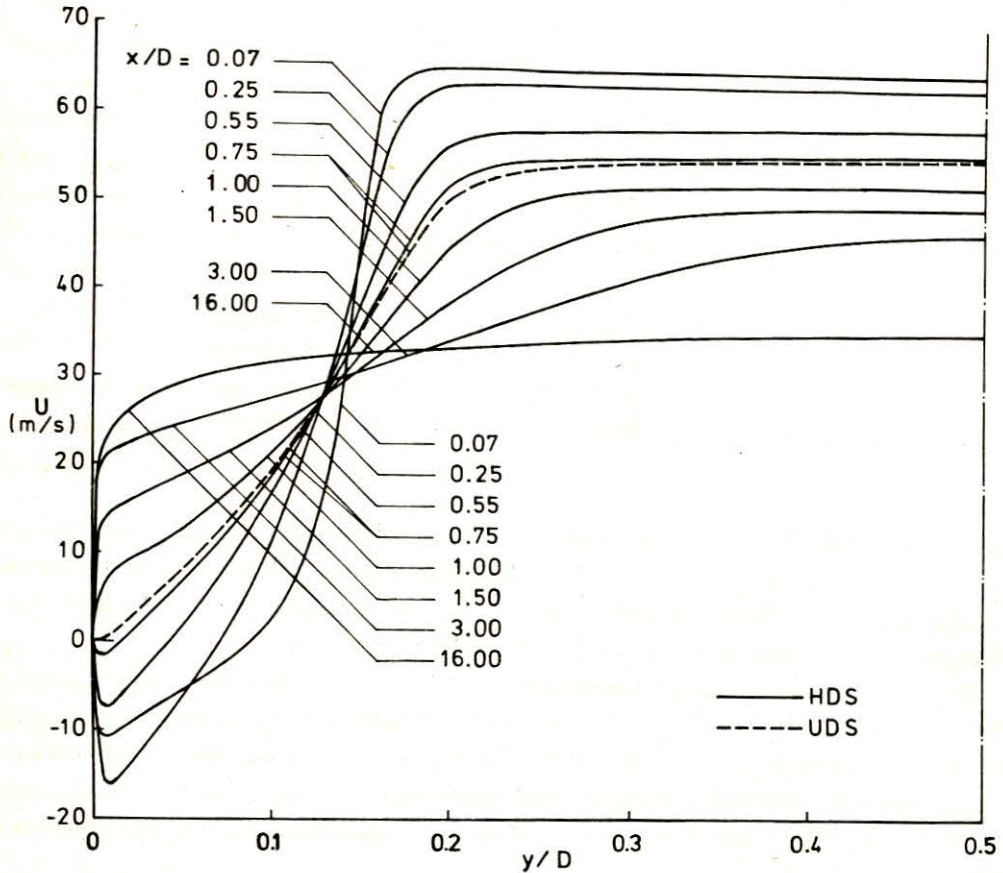

Figure 9 — Predicted radial profiles of axial velocity for axisymmetric sudden expansion of Moon and Rudinger[9]. Expansion ratio: $D/d = 1.428$.

sudden expansion pipe. Also shown in this figure is the predicted radial profile of axial velocity at x/D = 0.75 (dashed curve) obtained through the use of the UDS scheme. This figure is intended to show the development of the flow field as a function of the non-dimensional distance from the step, x/D. It can be seen that there is no flow reversal for x/D greater than about 0.75. It also may be noticed that the centre-line velocity decreases gradually with increasing distance from the step; thus, the flow from the smaller diameter pipe into the larger diameter one acts at first as if it were a free jet. At x/D = 3, the predicted centre-line velocity drops to 46.57 m/sec, while the experimental value reported by Moon and Rudinger[9] ise 38 m/sec. This indicates a difference of 8.57 m/sec between the predicted and measured values. However, it is reported that the estimated uncertainty in individual data points of Moon and Rudinger[9] could be as high as 4 m/sec. The velocity profile at x/D = 16 reveals that the velocity distribution approaches the shape of a fully developed turbulent flow.

Figure 10, which gives a comparison between the predicted and experimental radial profile of axial velocity at x/D = 0.75, shows that the predicted profile obtained with the HDS scheme is in better agreement with the experimental one than that obtained with the UDS scheme, moreover, the HDS scheme predicts a small recirculation near the wall, while the UDS scheme does not (see also Fig. 9). Furthermore,
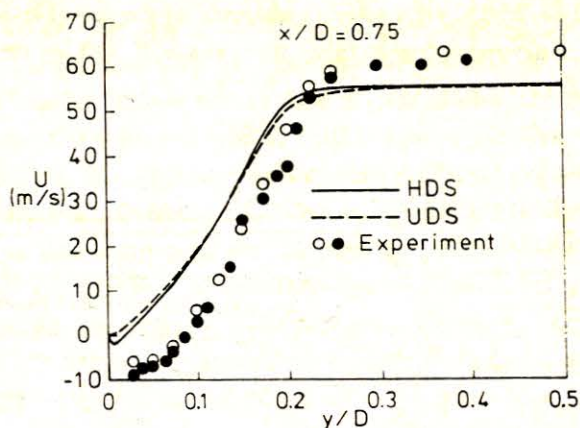

Figure 10 — Comparison of predicted radial profiles of axial velocity with experimental data of Moon and Rudinger[9] for an axisymmetric sudden expansion. Expansion ratio: D/d = 1.428.

this figure indicates that the predicted rate of spread of the round jet is too high, i.e., the recirculation zone thickness is too small. As stated in the first flow configuration above, the source of this problem is a limitation of the current k-ε turbulence model which does not account for the time lapse between extra turbulent energy being supplied and the effect being felt in the dissipating motions.

Figure 11 is a comparison of the predicted and experimental centreline velocity decay. As seen from the figure, the predicted decay in the initial region is faster and slightly slower downstream of the recirculation zone. It should also be noted that the HDS scheme gives better agreement with the experiment in the initial region than the UDS scheme; however, downstream of the recirculation zone both predictions coincide. In general, the agreement between the predicted and experimental decay of the centre-line velocity is qualitative.
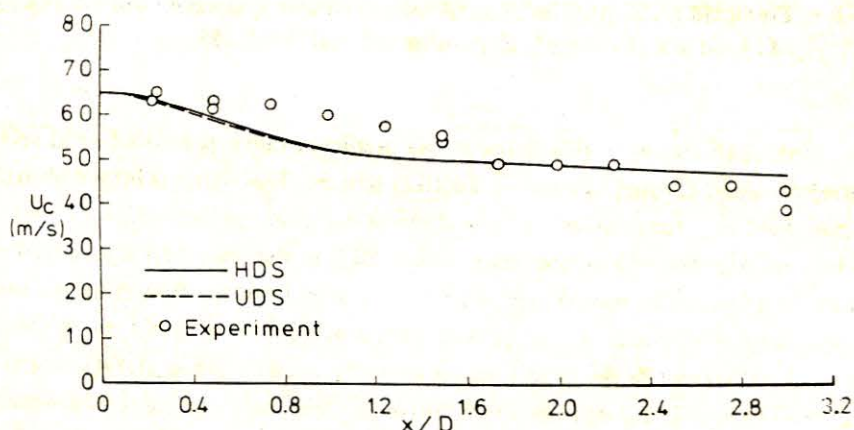

Figure 11 — Comparison of predicted centre-line velocity with experimental data of Moon and Rudinger[9] for an axisymmetric sudden expansion. Expansion ratio: D/d = 1.428.

4.4. Turbulent Flow Over a Backward-Facing Step

4.4.1. The physical situation considered

The physical situation considered is depicted in Fig. 3(c). It is a plane channel which has a step of height h and a total height of 3h; the expansion ratio being 3/2. A characteristic parameter governing the flow is the Reynolds number based on the step height h, and the mean axial velocity u_o upstream of the step, i.e., $Re_h = u_o h/v$. The flow over the backward-facing step was calculated for a Reynolds number of 3025.

4.4.2. Boundary conditions

With reference to Fig. 3(c), the boundary conditions for flow over a downstream-facing step here considered are as follows:

At the step inlet plane (i.e., $x/h = 0$) axial velocity distribution from measurements of Denham et al.[14] is prescribed, while the component of velocity in the y-direction is set to zero. The turbulence quantities k and ϵ are given uniform values (i.e., $k = 0.005\, u_o^2$, $\epsilon = C_\mu k^{3/2}/0.03(3h)$). At the step wall, velocity components u and v are set equal to zero. At the channel exit plane (i.e., $x/h = 29$), where the flow is parabolic, a condition of zero axial gradient is specified for all dependent variables (i.e., $\partial\phi/\partial x = 0$), while velocity component v is set to zero. At the top and bottom walls, u and v are set equal to zero.

As described in sub-section (4.2.2.), the turbulence quantities k and ϵ at the near-wall grid points are calculated employing the wall functions given in Section (2.3.).

4.4.3. Some computational details

For this flow situation, the finite-difference grid distribution is shown in Fig. 12. It consists of 32x21 grid points in the x- and y-directions, respectively; and its distribution in the respective directions in non-uniform, with more grid points located in the initial region and, in particular, in the region just behind the step where recirculation is present. Its length is 29h from the step.

For this grid employing the HDS scheme, a well-converged solution was obtained after 425 iteration cycles, and the computational time required was 9.53 min. on Pokey computer. As in the previous flow situations, the convergence criteria used were 10^{-3} for each equation. The under-relaxation factors employed in the computation for this problem were the same as those used in the computations for the previous problems given in sub-section (4.3.3.).
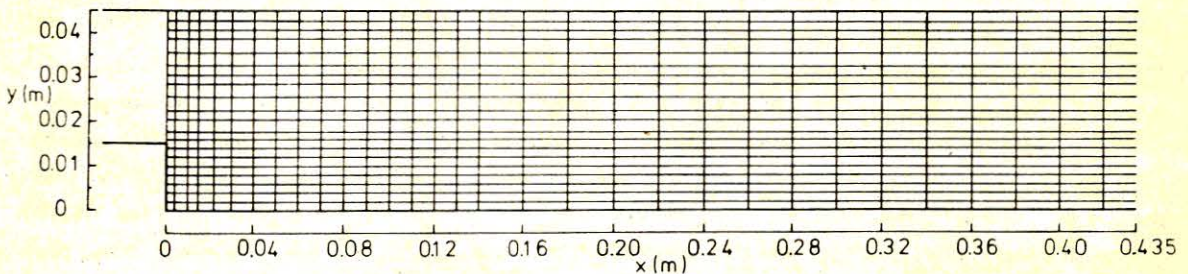

Figure 12 — Finite-difference grid distribution for flow over a backward-facing step.

4.4.4. Presentation and discussion of results

The predicted axial velocity profiles obtained using the HDS scheme and their comparison with the measurements of Denham et al.[14] for a Reynolds number of 3025 are displayed in Fig. 13, in non-dimensional form, u/u_o, at various axial locations, x/h. It can be seen from the figure, and as in the flow situations of sudden expansions in pipes of the previous case, that the predicted recirculation zone for flow over a backward-facing step is shorter in length and thinner in width than the experimental one. As described

in the previous case, the source of this problem is a limitation of the present k-ε turbulence model which does not account for the time lapse between extra turbulent energy being supplied and the effect being felt in the dissipating motions. However, the predicted profiles are seen to be in generally good agreement with the corresponding measured ones.

Computations were also made, with the same 32x21 grid size, employing the UDS scheme; however, the difference between the results of the two schemes was too small for a useful graphical comparison. For this reason the results obtained with the UDS scheme were not presented.
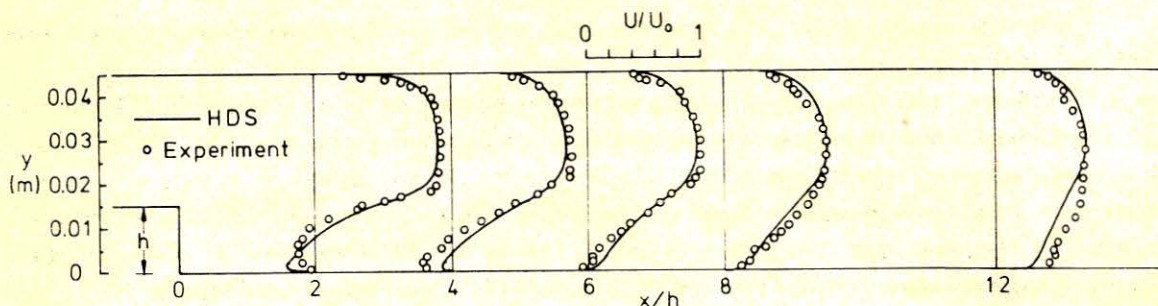

Figure 13 — Comparison of predicted axial velocity profiles with measurements of Denham et al[14].

5. CONCLUSIONS

The UDS and HDS discretisation schemes have been applied and evaluated successfully in the prediction of some turbulent flows in a variety of flow geometries.

In the case of developing turbulent flow through a pipe only the predictions made using the UDS scheme were compared with the experimental measurements of Barbin and Jones[7], since the predictions obtained employing the HDS scheme were exactly the same as those for the UDS scheme. The predicted developing axial velocity profiles and wall-shear stress distribution were found to be in good accord with the experimental measurements.

The calculations of the turbulent flow through sudden expansions in pipes were performed using both UDS and HDS schemes; it was found that the calculations obtained through the use of the HDS scheme were in closer agreement with experimental measurements procured by Chaturvedi[8], and Moon and Rudinger[9] that those obtained by the use of the UDS scheme. However, at downstream axial locations where there is a single predominant direction of motion, the results of calculations of both UDS and HDS schemes were seen to coincide. On the other hand, in the initial region where recirculation is present and where there is no single predominant direction of motion both UDS and HDS schemes predicted a recirculation zone which was shorter in length and thinner in width than the experimental one. The source of this problem is a limitation of the current k-ε turbulence model which does not account for the time lapse between extra turbulent energy being supplied and the effect being felt in the dissipating motions. In general, however, the predictions made for turbulent flow through axisymmetric sudden expansions in pipes using both UDS and HDS schemes were in good qualitative agreement with the experimental measurements.

In the case of turbulent flow over a backward-facing step, measurements for axial velocity profiles of Denham et al.[14] were compared with the axial velocity profiles obtained employing the HDS scheme only, since the axial velocity profiles obtained using the UDS scheme were essentially the same as those for the HDS scheme. The predicted axial velocity profiles were in generally good agreement with the corresponding measured ones. However, as in the case of turbulent flow through sudden expansions in pipes, the predicted recirculation zone behind the step was shorter in length and thinner in width than the experi-

mental one. The source of this problem, as in the flow through sudden expansions in pipes, is a limitation of the k-ε turbulence model. The model does not account for the time lapse between extra turbulent energy being supplied and the effect being felt in the dissipating motions.

REFERENCES

1. B.E. Launder and D.B. Spalding; Mathematical Models of Turbulence, Academic Press, London/ New York, 1972.
2. B.E. Launder and D.B. Spalding; "The numerical computation of turbulent flows", Comp. Meth. Appl. Mech. Engng., 3, 269-289 (1974).
3. J. Laufer; "The structure of turbulence in fully-developed pipe flow", NACA Rep. 1174 (1953).
4. C.J. Lawn; "The determination of the rate of dissipation in turbulent pipe flow", J. Fluid Mech., 48, 477-505 (1971).
5. J.W. Richman and R.S. Azad; "Developing turbulent flow in smooth pipes", Appl. Sci. Res., 28, 419-441 (1973).
6. C. Taylor, T.G. Hughes and K. Morgan; "A numerical analysis of turbulent flow in pipes", Int. J. Comp. and Fluids, 5, 191-204 (1977).
7. A.R. Barbin and J.B. Jones; "Turbulent flow in the inlet region of a smooth pipe", J. Basic Engng. Trans. A.S.M.E., 85, 29-34 (1963).
8. M.C. Chaturvedi; "Flow characteristics of axisymmetric expansions", Proceedings J. Hydraulics Division, A.S.C.E., 89, HY3, 61-92 (1963).
9. L.F. Moon and G. Rudinger; "Velocity distribution in an abruptly expanding circular duct", J. Fluids Engng. Trans. A.S.M.E., 99, 226-230 (1977).
10. B.T. Yang and M.H. Yu; "The flowfield in a suddenly enlarged combustion chamber", AIAA Journal, 21, 92-97 (1983).
11. A.S. Novick, G.A. Miles and D.G. Lilley; "Numerical simulation of combustor flow fields: A primitive variable design capability", J. Energy, 3, 95-105 (1979).
12. D.L. Rhode, D.G. Lilley and D.K. McLaughlin; "On the prediction of swirling flowfields found in axisymmetric combustor geometries", J. Fluids Engng. Trans. A.S.M.E., 104, 378-384 (1982).
13. D.L. Rhode, D.G. Lilley and D.K. McLaughlin; "Mean flowfields in axisymmetric combustor geometries with swirl", AIAA Journal, 21, 593-600 (1983).
14. M.K. Denham, P. Briard and M.A. Patrick; "A directionally-sensitive laser anemometer for velocity measurements in highly turbulent flows", J. Physics E: Scientific Instruments, 8, 681-683 (1975).
15. D.J. Atkins, S.J. Maskell and M.A. Patrick; "Numerical prediction of separated flows", Int. J. Num. Meth. Engng., 15, 129-144 (1980).
16. C.E. Thomas, K. Morgan and C. Taylor; "A finite element analysis of flow over a backward-facing step", Comp. and Fluids, 9, 265-278 (1981).
17. C. Taylor, C.E. Thomas and K. Morgan; "Modelling flow over a backward-facing step using the f.e.m. and the two-equation model of turbulence", Int. J. Num. Meth. Fluids, 1, 295-304 (1981).
18. J. Kim, S.J. Kline and J.P. Johnston; "Investigation of a reattaching turbulent shear layer: Flow over a backward-facing step", 102, 302-308 (1980).
19. P.J. Roache; Computational Fluid Dynamics, Hermosa Publishers, Albuquerque, N.M., 1976.
20. S.V. Patankar; Numerical Heat Transfer and Fluid Flow, McGraw-Hill Book Company, New York, 1980.
21. D.B. Spalding; "A novel finite-difference formulation for differential expressions involving both first and second derivatives", Int. J. Num. Meth. Engng., 4, 551-559 (1972).

22.   S.V. Patankar and D.B. Spalding; "A calculation procedure for heat, mass and momentum transfer in three-dimensional parabolic flows", Int. J. Heat Mass Transfer, 15, 1787-1806 (1972).

23.   L.S. Caretto, A.D. Gosman, S.V. Patankar and D.B. Spalding; "Two calculation procedures for steady, three-dimensional flows with recirculation", Proc. 3rd Int. Conf. Num. Methods Fluid Dyn., Paris, 11, 60-68 (1972).

24.   W.M. Pun and D.B. Spalding; "A general computer program for two-dimensional elliptic flows", Rep. HTS/76/2, Imperial College, London, 1976.

25.   T. Karasu; "Numerical prediction of incompressible turbulent swirling flows in circular-sectioned ducts and annuli", Ph. D. Thesis, University of London, 1981.

26.   M.A. Leschziner; "Practical evaluation of three finite difference schemes for the computation of steady-state recirculating flows", Comp. Meth. Appl. Mech. Engng., 23, 293-312 (1980).